PRELIMINARY NEUTRONIC ANALYSES OF THE TRIGA-ADS DEMONSTRATION FACILITY

C. Rubbia, M. Carta, N. Burgio, C. Ciavola, A. D'Angelo, A. Dodaro, A. Festinesi, S. Monti, A. Santagata and F. Troiani
ENEA
ENEA/C.R. Casaccia, via Anguillarese, 301, 00060 S. Maria di Galeria (Roma), Italy
presidenza@sede.enea.it; carta@casaccia.enea.it; burgio@casaccia.enea.it; ciavola@casaccia.enea.it; dangelo@casaccia.enea.it; alessandro.dodaro@casaccia.enea.it; armando.festinesi@casaccia.enea.it; monti@bologna.enea.it; alfonso.santagata@casaccia.enea.it; troiani@saluggia.enea.it

M. Salvatores and M. Delpech
CEA
CEA/Cadarache, 13108 Saint-Paul-Lez-Durance, France
salvatores@drncad.cea.fr; marc.delpech@cea.fr

Y. Kadi, S. Buono, A. Ferrari, A. Herrera Martínez and L. Zanini
CERN
CERN/European Organization for Nuclear Research, CH - 1211 Geneva 23, Switzerland
yacine.kadi@cern.ch; stefano.buono@cern.ch; alfredo.ferrari@cern.ch; adonai.herrera.martinez@cern.ch; luca.zanini@cern.ch

G. Imel
ANL
Current address: CEA/Cadarache, 13108 Saint-Paul-Lez-Durance, France
imel@anl.gov

ABSTRACT

TRADE (TRiga Accelerator Driven Experiment), to be performed in the TRIGA reactor of the ENEA-Casaccia Centre (Italy), consists in the coupling of an external proton accelerator to a target to be installed in the central channel of the reactor scrammed to sub-criticality. This pilot experiment, aimed at a global demonstration of the ADS concept, is based on an original idea of Carlo Rubbia. The present paper reports the results of some neutronic analyses focused on the feasibility of such experiment. Results show that all relevant experiments (at different power levels in a wide range of sub-criticalities) can be carried out, with relatively limited modifications to the present TRIGA reactor.

1. INTRODUCTION

In the European Roadmap towards the experimental demonstration of ADS [1], several experiments are indicated which should allow to validate the separate components of such systems. The coupling of the components will be performed in a new system, with all innovative features included, with the exception of the sub-critical core fuel, which should be of a well-proven type. However, the case for the licensing of such a

system can present some difficulty, in absence of a preliminary coupling experiment at power. A way out is simply to realise an experiment where an "existing" (low) power reactor, with well-known safety features, is made sub-critical and coupled with an accelerator, which should provide the needed protons to induce spallation reactions on a target hosted inside the core.
As far as coupling, such experiment will not need a high neutron yield from spallation. In fact it could be run even with a neutron per proton production rate as low as one, since an optimisation in terms of efficiency or transmutation will not be a requirement.
The domain of interest of such experiment will be to show a reliable operation of the system, from start-up to nominal power level, up to shutdown, in presence of thermal reactor feedback effects. The presence of control rods in the system will allow to verify different modes of operation during fuel irradiation and the determination and monitoring of reactivity levels with "ad-hoc" techniques.
The possibility to run the experiment at different levels of sub-criticality (realised e.g. with appropriate fuel loading patterns), will allow to explore experimentally the transition from an "external" source-dominated regime, to a core thermal feedback-dominated regime. This transition is relevant, in particular to understand the dynamic behaviour of an ADS, which, in the future full scale demonstrations of transmutation, could have both a very low β_{eff} and very low Doppler reactivity effect.
C. Rubbia suggested that this pilot experiment, which would be the first example of ADS components coupling "at real size", could be carried out on the TRIGA reactor at the ENEA Casaccia Centre (Italy), an existing pool reactor of 1 MW thermal power, cooled by natural convection of water in the reactor pool.
The TRADE (TRiga Accelerator Driven Experiment) project is based on the coupling of an upgraded proton cyclotron with the TRIGA reactor in a sub-critical configuration. The flexibility offered by the pool reactor is eminently suited for the conversion into the sub-critical configuration, which is achieved through:

- The removal of the innermost fuel ring of the core.
- The loading/unloading of the outermost fuel ring rods of the core to attain, by small reactivity steps, the desired sub-criticality level.

The spallation target will consist of solid tungsten. The target should be hosted in the central thimble, at present used for high neutron flux irradiation. The target performances can be limited by the geometry of the irradiation channel: notwithstanding an adequate power (few tens kW up to 50÷80 kW) should be possible to be achieved in the target.
A core power of several hundreds kW is needed in order to explore the dynamics, reactivity control and power monitoring in an ADS, in the subcriticality range ranging from source dominated to reactor feedback dominated regime, e.g. from k=0.9 to k=0.99 or more. The use of protons of about 100 MeV is suggested by considerations on maximum power (which can be evacuated in the solid tungsten target), accelerator cost and minimum size of the bending magnets needed to introduce the beam inside the core (see next Section where the calculation model of the whole system is reported). With these parameters (i.e. about 500 kW in the core, 50 ÷80 kW in the target, subcriticality as low as k = 0.9 and proton energy E_p = 100 MeV), one has the requirement for a maximum proton current value of about 500 μA.
In terms of neutron spectrum type, it has been shown that the TRIGA thermal spectrum allows to perform experiments representative also of a fast neutron spectrum. In fact, although the kinetic parameters of TRIGA and of fast neutron spectrum are very different, the kinetic response to perturbations is identical, except for a shifting to the lower frequencies of the reactor transfer function. This feature allows to investigate and validate the dynamic behaviour of an ADS, rather independently from the neutron spectrum [2]. Moreover, the TRADE experiment, that can be seen also as a successive step with respect to the MUSE [3] experiments (fast spectrum), will benefit from the extensive experimental techniques development performed in this last experimental program.
The present paper gives preliminary results about the neutronics of selected possible configurations, the radiological impact of TRADE (results concerning some particular shielding analyses have been recently presented in a dedicated paper [4]), and the activation of the target/beam-line components. Monte Carlo simulation codes were used (FLUKA and EA-MC [5, 6] at CERN, and MCNP-4C [7] at ENEA/Casaccia) for static and burnup/evolution analyses. A simple tool, obtained by coupling a core channel time dependent thermal-hydraulics code with a neutron point-kinetics code, was used to perform some preliminary dynamic analyses (TIESTE-MINOSSE [8] at ENEA/Casaccia).

2. MONTE CARLO CALCULATION METHODS

The sequence of phenomena from high-energy protons induced cascade in a heavy-Z material (lead or tungsten), producing neutrons that subsequently interact until they are finally absorbed or escape, is rather complex. For a correct simulation of TRADE, it is essential to understand the fine details of the physics related to all these phenomena. In order to do so, innovative simulation codes were used (FLUKA and EA-MC [5, 6] at CERN, and MCNP-4C [7] at ENEA/Casaccia), which stochastically calculate the distribution of neutrons in three-dimensional space as a function of energy and time[1]. These codes allow the description of complex geometrical models. Special attention was devoted to the development of techniques (for kinematics calculation, cross-section evaluation, importance biasing, etc.) to minimize the computer time in order to provide sufficient statistics.
The design of ADS requires powerful simulation tools for:

- The modelling of the high-energy cascade and of the neutron production.
- The transport of the low energy ($E \leq 20$MeV) neutrons.
- The description of the fuel evolution as a result of neutron interactions and nuclear decays.
- The nuclear transmutation and activation of the structural materials and coolant due to the presence of a neutron fluence and of the proton beam induced high-energy cascade.

Standard analysis routes developed for critical nuclear reactors cannot be applied immediately to externally driven sub-critical systems and to TRADE in particular. Indeed, the spatial distribution of the neutron flux is expected to be radically different in the two cases. While in a critical reactor the flux distribution inside the volume is determined essentially by the boundary conditions, in an ADS the effect of the initial high-energy cascade is dominant. In fact, in a sub-critical arrangement the neutron flux along any radial direction starting from the centre must fall-off in an approximately exponential manner. The corrections to the exponential behaviour depend primarily on the shape of the source and they are important when close to it.
A refined modelling of the TRADE experiment was implemented. Figure 1 shows the calculation model for the TRADE analysis by FLUKA and EA-MC.

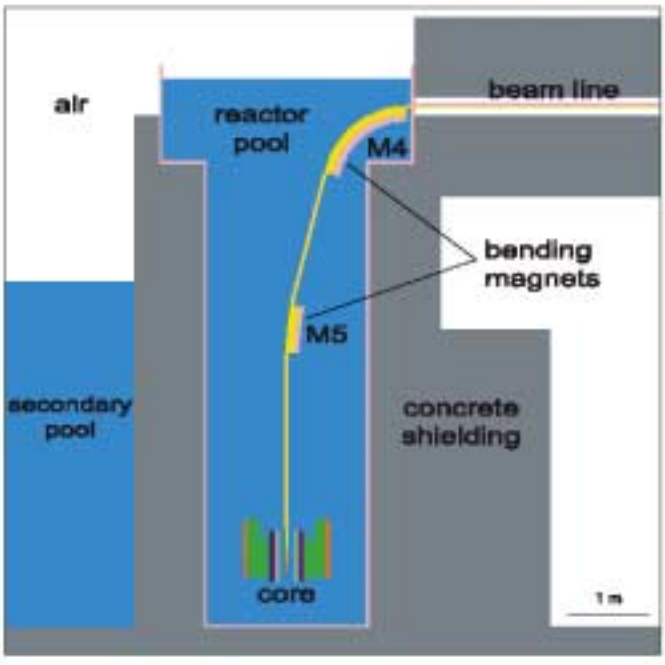

Figure 1 - Schematic view of the implemented model.

[1] A special feature of EA-MC is to perform, in an integrated way, refined evolution calculation.

3. GENERAL CHARACTERISTICS OF THE NOMINAL TRIGA CORE

The TRIGA core consists of an annular structure immersed in water, which serves as primary coolant. The core is arranged in a honeycomb-like array forming an annulus with six coaxial cylindrical rings of fuel elements (Figure 2).

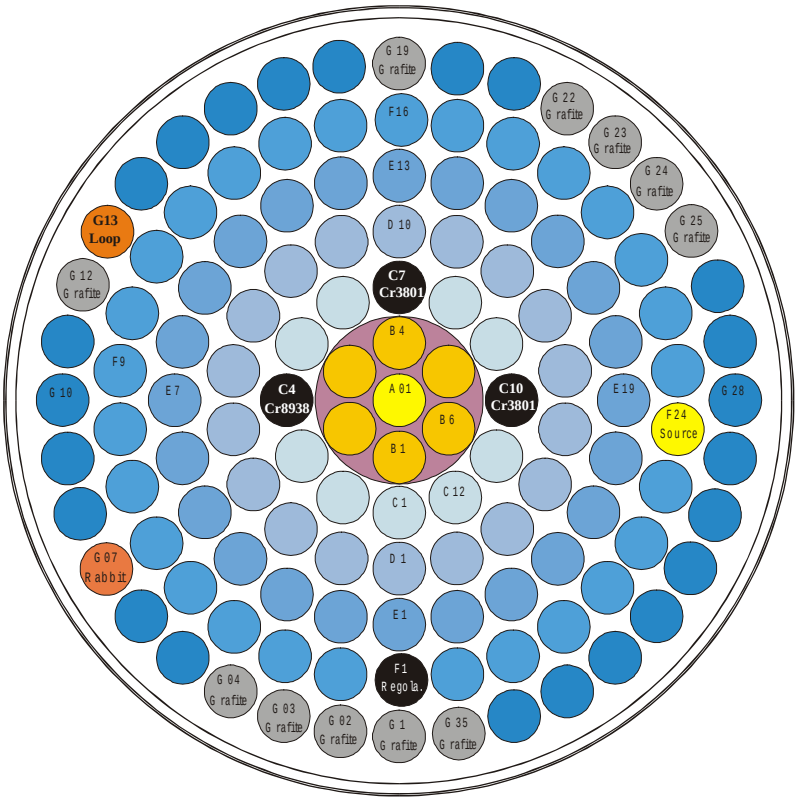

Figure 2 - Schematic view of the TRIGA core.

The core, which is surrounded by the graphite reflector, consists of a lattice of fuel elements, graphite dummy elements, control and regulation rods. There are 127 channels divided in seven concentric rings (from 1 to 36 channels per ring). The channels are loaded with fuel rods (blue elements in Figure 2), regulation and control rods (black elements in the figure) depending on the power level required, graphite dummies (grey elements) and a central thimble for high flux irradiations (element A01), plus supplementary experimental channels.
The diameter of the core is about 56.5 cm while the height is 72 cm. Neutron reflection is provided by graphite contained in an aluminium container, which is surrounded by 5 cm of lead acting as a thermal shield. The reactor core is cooled by natural convention of the water in the reactor pool.
The fuel element has an external diameter of 3.73 cm (clad included) and a total height of 72 cm (Figure 3).

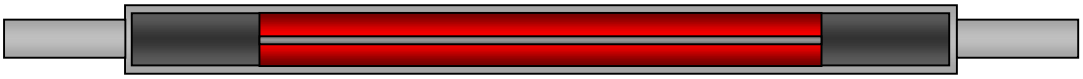

Figure 3 - Fuel rod section (scale ≈ 1:5)

The fuel is a cylinder (38.1 cm high, 3.63 cm in diameter) of Uranium-Zirconium-Hydrogen ternary alloy (1.7:1 H/Zr atom ratio and 8.5 wt% of Uranium 20 wt% enriched in ^{235}U) with a metallic zirconium rod inside. There are two graphite cylinders at the top and bottom of the fuel rod. The regulation rod has the same morphological aspect as the fuel rod, with the exception that the fuel is replaced by the absorber (graphite with powdered boron carbide). The control rods are "fuel followed" with geometry similar to that of the regulation rod.

4. SUBCRITICAL CORE CONFIGURATIONS

4.1 FUEL RODS AND CONTROL RODS REACTIVITY WORTH

The analyses aimed to draw a first picture about the modularity of the TRIGA reactor concerning different fuel rod (FR) sub-critical configurations and control rod (CR) arrangements. The nominal (reference) configuration for the analyses (Figure 2) was characterized by the central thimble (that should host the target), 108 FR and 3 CR. Table I shows the results concerning different hypothesis about the fuel loading and the CR insertion level and positions. In particular, the following situations were taken into account with respect to the nominal configuration: concerning FR, no ring B in the core (shadowed central zone in Figure 2), with water replacing fuel, and no rings B and G in the core, with fuel in ring G replaced by graphite elements; concerning CR, elements were positioned in ring C, as in the nominal configuration, or positioned in ring D, with different insertion levels (critical relative to the nominal loading, completely withdrawn or fully inserted).

Table I - FR and CR reactivity worth.
(↔ = CR at critical insertion for the nominal fuel loading, ↑ = CR completely withdrawn, ↓= CR fully inserted)

Fuel Rods loading	Control Rods insertion level and position	**20 W** ΔK/K (pcm)		**200 kW** ΔK/K (pcm)		**500 kW** ΔK/K (pcm)	
		To criticality	CR Worth	To criticality	CR Worth	To criticality	CR Worth
Nominal	↑ in ring C	+4390	-8280	+3800	-8280	+2950	-8280
	↓ in ring C	-4250		-4790		-5570	
Without ring B	↔ in ring C	-4630		-4860		-5030	
	↑ in ring C	-1360	-6440	-2070	-6440	-2740	-6440
	↓ in ring C	-7710		-8380		-9000	
	↑ in ring D	-1360	-6660	-2070	-6660	-2740	-6660
	↓ in ring D	-7930		-8590		-9220	
Without rings B and G	↔ in ring C	-9040		-9070		-9120	
	↑ in ring C	-4180	-8060	-5800	-8060	-6580	-8060
	↓ in ring C	-11900		-13390		-14110	
	↑ in ring D	-4180	-7590	-5800	-7590	-6580	-7590
	↓ in ring D	-11450		-12950		-13670	

Three power levels (each one with different CR insertion levels into the core at criticality) were taken into account: 20 W, 200 kW and 500 kW (respectively, T_{fuel} =27 °C, 114 °C and 174 °C in calculations). In Table I, FR (negative) worths in ring B were calculated with respect to water (water minus fuel), whereas FR ring G worths were calculated with respect to graphite (graphite minus fuel). CR worths were calculated with respect to the fuel follower. As already mentioned, the critical insertion level for CR in Table I (indicated as ↔) is relative to the nominal fuel loading
Concerning the different fuel loadings of the core, results show:

- The FR worth in ring B depends on the CR level insertion (for example, at 20 W, FR ring B worth is +4390-(-1360)=+5750 pcm with CR ↑ positioned in ring C against -4250-(-7710)=+3460 pcm with CR ↓). In particular, it is maximum with CR withdrawn from the core (FR in ring B are well coupled with the core) and minimum with CR fully inserted into the core (FR in ring B are less coupled with the core).
- The FR ring G worth, without FR in ring B, depends on the CR level insertion (for example, at 20 W, FR ring G worth is -1360-(-4180)=+2820 pcm with CR ↑ positioned in ring C against -7710-(-11900)=+4190 pcm with CR ↓). In particular, it is minimum with CR withdrawn from the core (less importance of the core peripheral zones) and maximum with CR fully inserted into the core (more importance of the core peripheral zones).
- The FR ring G worth, without FR in ring B, is smaller with CR fully inserted in ring D with respect to the situation with CR fully inserted in ring C (for example, at 20 W, FR ring G worth is -7710-(-11900)=+4190 pcm with CR ↓ positioned in ring C against -7930-(-11450)=+3520 pcm with CR ↓ positioned in ring D).

Concerning control rods, results show:

- CR worths are practically independent on the power level: for this reason, mean values among different power levels are quoted in Table I.
- CR worths are smaller without FR in ring B (CR positioned at the internal boundary of the core), and increase without FR in rings B and G (core more compact).

As a general point of view, TRADE seems to offer a variety of suitable sub-critical loadings. At a first glance, one loading could be with FR ring B removed from the core and with CR positioned in ring D. In such a case, the target value K_{eff} 0.97 ÷ 0.98 can be attained with CR in ring D completely withdrawn from the core (safe condition), and tuning the K_{eff} value by progressive loading (or unloading) of the FR in ring G. It should be noted that, though removing FR ring B from the core decreases CR worths, at cold condition (20 W) the sub-criticality level with CR inserted (about -7700 ÷ -7900 pcm depending on the CR positioning) is almost twice the reference value (- 4250 pcm, second row in Table I) calculated for the current TRIGA layout.
Figure 4 shows the behaviour of K_{eff} as a function of the number of fuel elements loaded (CR completely withdrawn from the core).

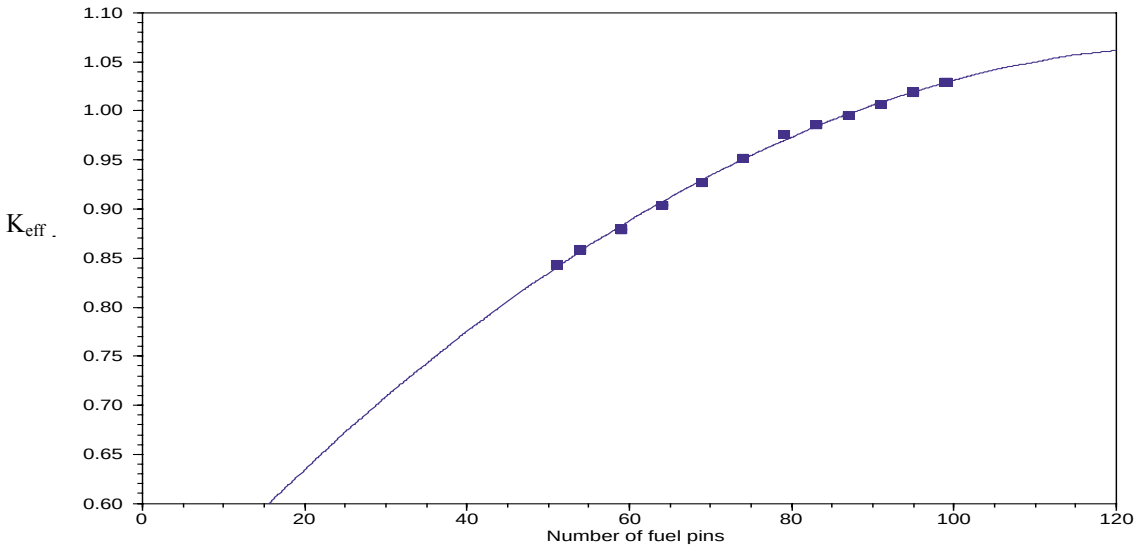

Figure 4 - K_{eff} behaviour as a function of the fuel loading.

4.2 POWER AND TEMPERATURE COEFFICIENTS

Concerning power and temperature coefficients, from the first row of Table I (nominal fuel loading with CR withdrawn in ring C), the following values can be derived: about -3.0 pcm/kW (–6.8 pcm/°C in terms of medium temperature rise in the core) going from 20 W to 200 kW, and about –2.8 pcm/kW (-14.2 pcm/°C) going from 200 kW to 500 kW. Reactivity insertion measurements made during the first Casaccia TRIGA tests have been analysed by the TIESTE-MINOSSE code [8]. The TIESTE-MINOSSE code is a simple tool developed at ENEA by coupling a core channel time dependent thermal-hydraulics code with a neutron point-kinetics code. The resulting fuel feedback features have been compared with statically measured temperature and power coefficients, obtained by measuring both the fuel temperature and the reactivity of a calibrated control rod at different power levels. The comparison shows a significant agreement between the above-mentioned analysis of TRIGA dynamics and the more recent power coefficient static measurements. Figure 5 shows a first temperature coefficient "linear fit" function used in the dynamic code to analyse the available experimental results. The same plot shows the results obtained by the preliminary Monte Carlo calculations (first row of Table I).

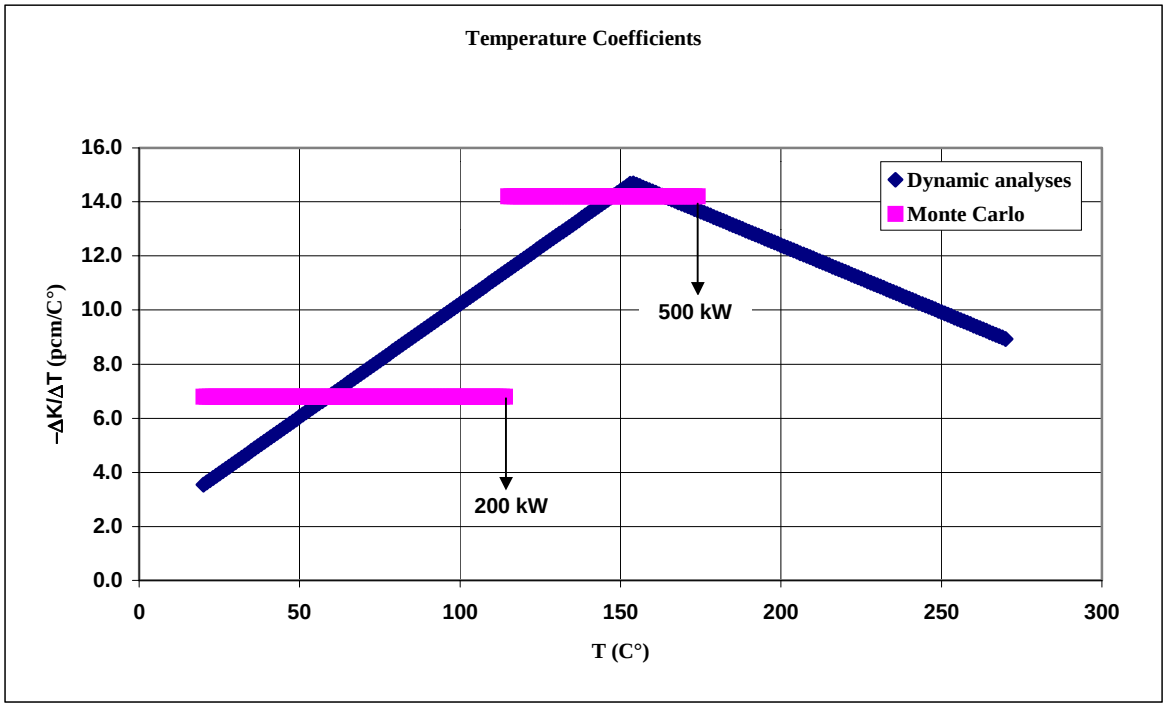

Figure 5 - TRIGA temperature coefficients analysis.

4.3 CORE SPATIAL DISTRIBUTION OF THE NEUTRON FLUX

The power distribution in a sub-critical system is sensitive to the core intrinsic multiplication factor. As the latter increases towards unity (criticality conditions), the neutron flux distribution flattens on the core fundamental harmonic. Figures 6 and 7 show the radial flux distribution averaged over the channels of a given cylindrical ring and the axial flux distribution for the hottest fuel pin respectively, for different sub-criticality levels. Neutron flux is normalized at 1 MW_{th} thermal power. Different rings positions are also indicated in Figure 6.

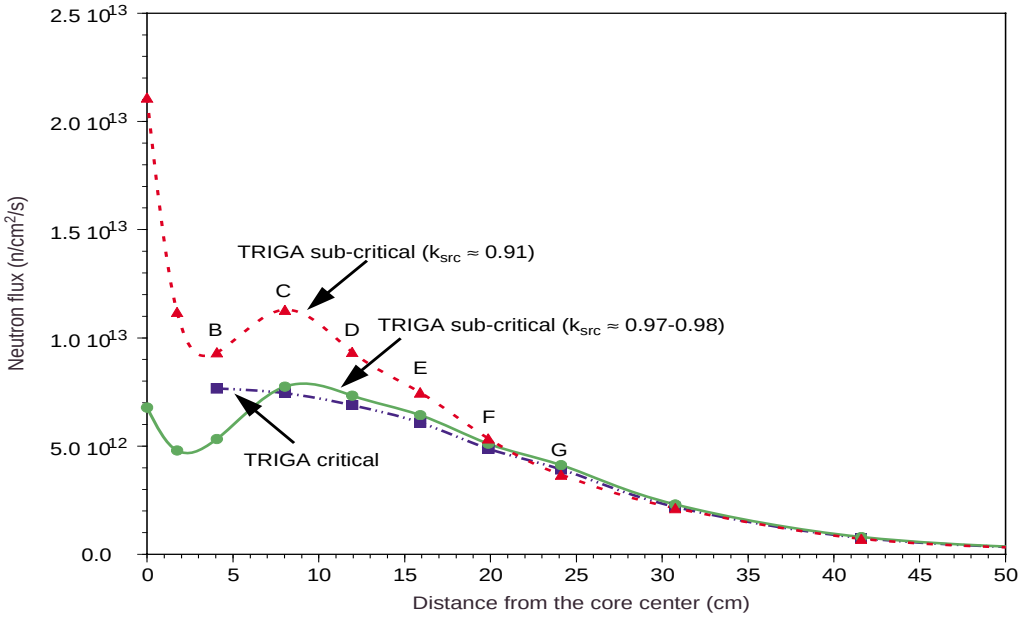

Figure 6 - Radial distribution of the neutron flux in the TRIGA core.

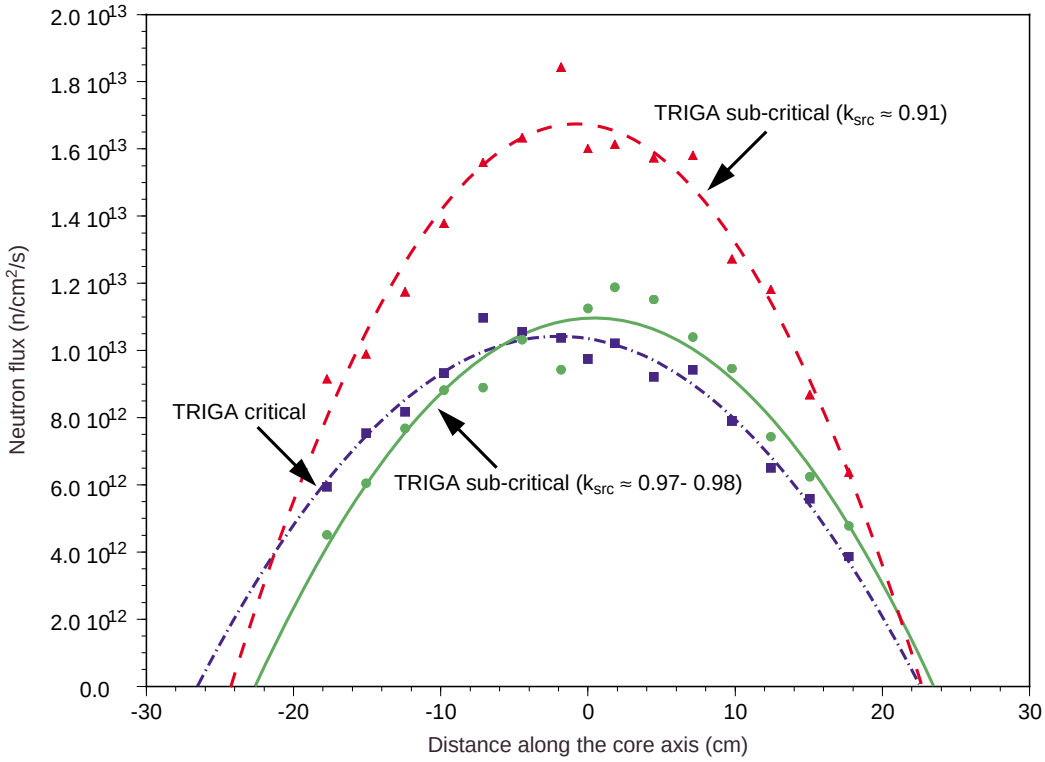

Figure 7 - Axial distribution of the neutron flux in the hottest fuel pin.

It is worth noting that despite the large sub-criticality margin, the radial and axial power profiles have a moderate peaking factor (see also Section 5). This implies that, in a first approximation, the thermal-hydraulic properties of the core are compatible with a presence of an intense spallation neutron source in the central channel.

5. GLOBAL NEUTRONIC PARAMETERS

Three sub-critical core configurations, operated at 200 kW_{th}, have been chosen for the initial feasibility study phase:

(i) A reference configuration consisting of 102 fuel rods (nominal configuration as in Section 3 without fuel rods in ring B and with the 3 control rods withdrawn, i.e. fuel follower inserted) resulting in a $K_s \approx 0.97 \div 0.98$ (see below for the definition of K_s).
(ii) A second configuration consisting of 107 fuel rods (same as (i) with 5 additional fuel rods in ring G) resulting in a slightly sub-critical core, i.e. $K_s \approx 0.99$.
(iii) A third configuration consisting of 79 fuel rods (nominal configuration as in Section 3 without fuel rods in rings B and G, and with the 3 control rods at critical level, resulting in a deep sub-critical core, i.e. $K_s \approx 0.90$.

For the sake of comparison, the nominal configuration has been included. The main global results of the three TRIGA sub-critical configurations, in addition to the critical case, are summarised in Table II.

Table II - Main parameters of the TRIGA sub-critical configurations.

Global Parameters	Symbol	Reference case	Critical	High K_s	Low K_s
Thermal Power Output	P_{th} (kW)	200	200	200	200
Proton Beam Energy	E_p (MeV)	110	—	110	
Spallation Neutron Yield	$N_{(n/p)}$ (n/p)	0.451	—	0.451	
Neutron multiplication	M_s	44.1	—	84.1	10.4
Multiplication Coefficient	$K_s=(M_s-1)/M_s$	0.977	1.000	0.988	0.903
Energetic Gain	G	15.1	—	28.1	4.0
Gain coefficient	G_0	0.34	—	0.33	0.39
Accelerator Current	I_p (mA)	0.13	—	0.07	0.61
Beam Power	P_{beam} (kW)	14.2	—	7.4	66.9
Core Power Distributions					
Av. Fuel Power Density	P_{th}/V_{fuel} (W/cm^3)	4.9	4.8	4.7	6.5
Max. Linear Power	P_l (W/cm)	75.6	70.2	70.5	118.2
Radial Peaking Factor	P_{max}/P_{ave}	1.48	1.45	1.46	1.76
Linear Peaking Factor	P_{max}/P_{ave}	1.51	1.45	1.48	1.78

M_s indicates the net multiplication factor in the presence of an external source. Table II reports a source multiplication coefficient K_s, formally defined as $K_s = 1\text{-}1/M_s$, of 0.977 for the reference configuration, which is different in general from the effective neutron multiplication factor, K_{eff}. This value has been chosen in such a way that criticality conditions are prevented, with adequate margins, under all normal conditions as well as following transient and accident conditions.
The main neutronic parameters for the different source configurations are shown in Table III.

Table III - Main neutronic parameters for the different source configurations.

	Reference	High K_s	Low K_s
K_s	0.977	0.988	0.903
K_{eff}	0.974	0.988	0.894
φ^*	1.142	1.035	1.110

Where φ^* is the importance of source neutrons, defined as:

$$\varphi^* = \frac{\nu}{\nu'} \cdot \frac{(1-K_{eff})/(K_{eff})}{(1-K_s)/(K_s)}$$

The EA-MC code allows for the straightforward production of neutron flux spectra at selected locations. Figure 8 shows some spectra, which allows further insight into the neutronic characteristics of the device.

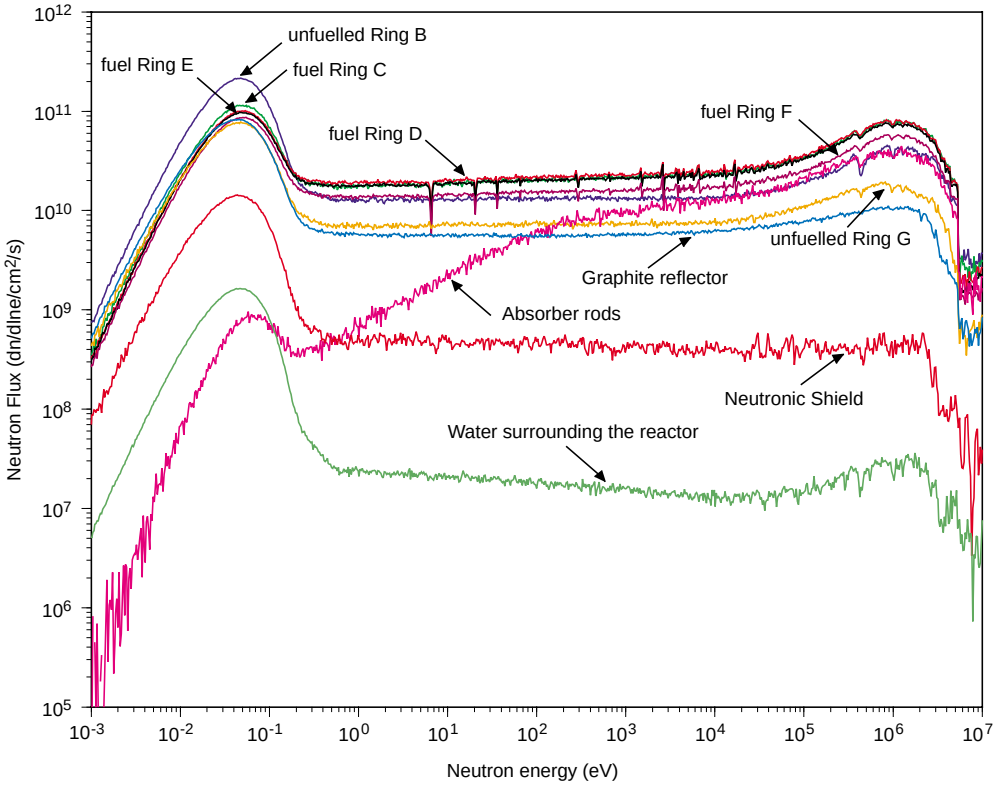

Figure 8 - Neutron flux spectra at selected locations of TRADE reference configuration.

A detailed inventory of the neutron induced reactions taking place in several locations of the device is given in Table IV.

Table IV - Neutron reaction inventory at several locations of TRADE reference configuration.

Neutron Absorption Inventory		**Neutron Absorption Inventory**	
Reactor vessel	.002 %	Absorber rods	6.44 %
Neutron shield	1.04 %	Cladding	10.47 %
Aluminiun lining	1.46 %	Fuel ring C	7.91 %
Upper grid	0.05 %	Fuel ring D	14.55 %
Lower grid	0.08 %	Fuel ring E	18.45 %
Spallation target	0.18 %	Fuel ring F	18.64 %
Primary coolant	19.82 %	Fuel total	59.55 %
Core radial reflector	0.79 %	Escapes	0.05 %
Core axial reflector	0.07 %	Total	100 %
Main Nuclear Reactions		**Main Nuclear Reactions**	
Capture	53.06 %	Others	7.00 %
Fission	38.85 %	Escapes	0.05 %
n,Xn	1.04 %	Total	100 %

6. RADIOLOGICAL IMPACT OF TRADE

An essential role in the feasibility study of the experiment is played by radioprotection calculations. In fact, such a system exhibits new characteristics with respect to a traditional reactor, due to the presence of the intense proton accelerator. Therefore one needs to perform shielding studies not only around the reactor core but also along the beam line, with particular attention paid to the permanent magnets, which drive the protons towards the core of the TRIGA reactor. Beam losses are always present in the normal operating condition of an accelerator, and the effective dose in these conditions must be evaluated. In addition, several accident cases related to the failure of the accelerator should be considered.

We describe the results from detailed Monte Carlo (MC) transport calculations (Figure 1) performed in the course of this analysis: neutrons streaming in the reactor building from the vessel and analysis of their energy spectra; spallation neutrons produced in the case of the proton beam colliding against the bending magnet M4; radiation dose in the case of normal beam losses. Shielding against these contingencies was also designed and analysed through the same methods.

6.1 HIGH-ENERGY BEAM TARGET INTERACTIONS

The distribution of neutrons generated in the spallation target unit (tungsten rod) and surrounding core structures is given in Figure 9. Spallation neutrons are produced in a region extending radially up to 5 cm from the center of the core, that is a few cm before reaching the fuel elements. Their average kinetic energy is of the order of 3 ÷ 4 MeV. These neutrons are rapidly slowed down by the water moderator before reaching the core internal structures, therefore they do not represent a major problem in terms of radiation damage. It is worth noting that a few thermal neutrons, up to 10^9 n/cm^2/s/mA, will stream along the beam tube and slightly irradiate (1.3×10^{-5} Gy/s/mA) the lower permanent magnet (M5 - Figure 1), situated 3 m above the core. These detailed MC calculations (involving importance biasing techniques) show that the neutron leakage through the top of the reactor pool is negligible.

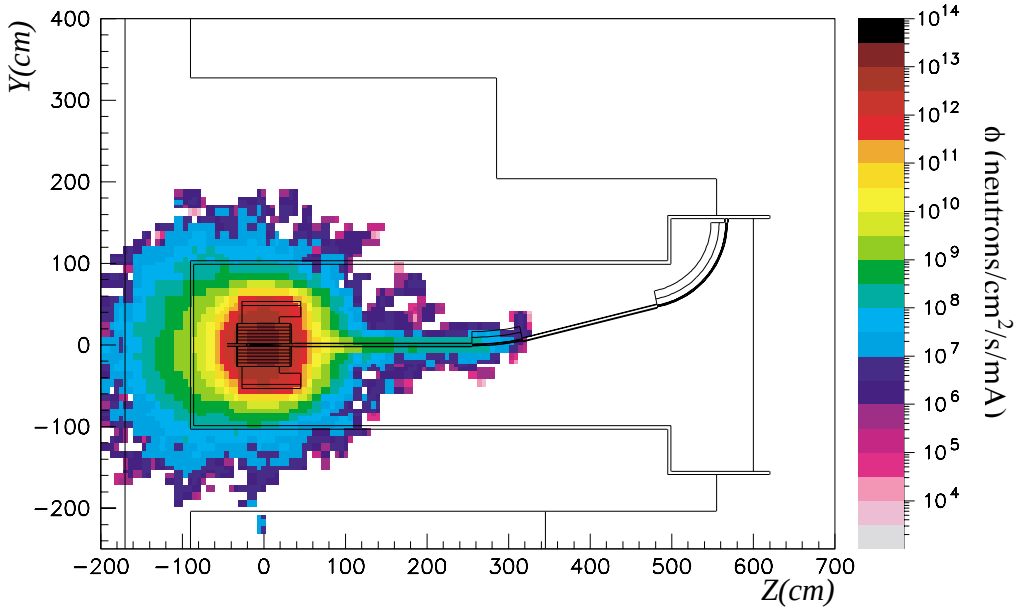

Figure 9 -Neutron flux distribution (n/cm^2/s/mA) following the impact of 110 MeV protons on a solid tungsten target.

However, this is not the case for photons generated by nuclear interactions which propagate mostly through the water moderator (Figure 10), although only a small fraction reach the surface of the reactor pool (10^4 $\gamma/cm^2/s/mA$).

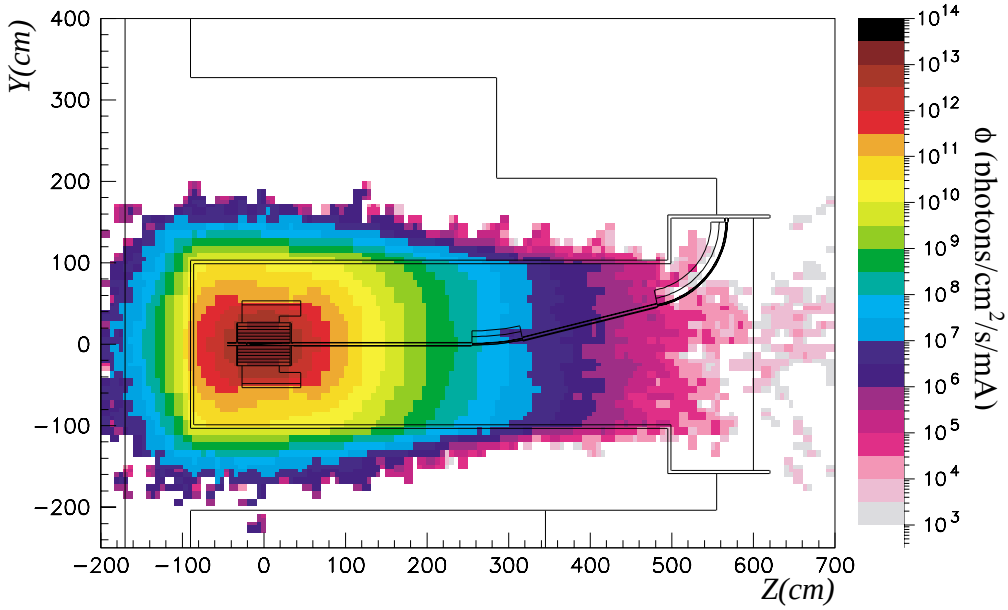

Figure 10 - Photon flux distribution ($\gamma/cm^2/s/mA$) following the impact of 110 MeV protons on a solid tungsten target.

6.2 SHIELDING ASPECTS OF THE PROTON BEAM LINE

One of the main worries associated with the coupling of the accelerator and the TRIGA reactor is the radiation produced during normal operation, due to protons escaping along the beam line. These losses should be of the order of $10^{-4} \div 10^{-6}$ of the beam current, i.e. between 1 and 100 nA/m, which implies, integrating over time, a large amount of radiation produced. Taking into account the maximum allowable dose rate in the accessible area of the reactor building (10 μSv/h), significant shielding will be required. Several shielding options were considered based on the nature and the thickness of the concrete used. We report here the main results from these calculations.

We consider first the case in which all the protons exit the beam line interacting with the beam pipe and the shielding. This case would correspond to the failure of one of the focusing quadrupoles. In order to calculate the doses due to normal beam losses, it is sufficient to re-scale the results by a factor of 10^{-5} (1 nA/m along 10 m) which corresponds to the beam losses along the straight part of the beam line.

The distribution of the particles generated in the beam tube and the surrounding concrete (baryte) shielding as a result of the interactions produced by the protons exiting the beam line is given in Figure 11. Spallation neutrons are produced in the aluminium beam tube (8 mm thick) with a yield of ~ 0.03 n/p and as deep as 1 m inside the concrete (~ 0.14 n/p, that is 82% of the neutrons produced) due mainly to high-energy neutrons interacting with the heavy nuclides present in concrete, such as barium (8% of the atoms).

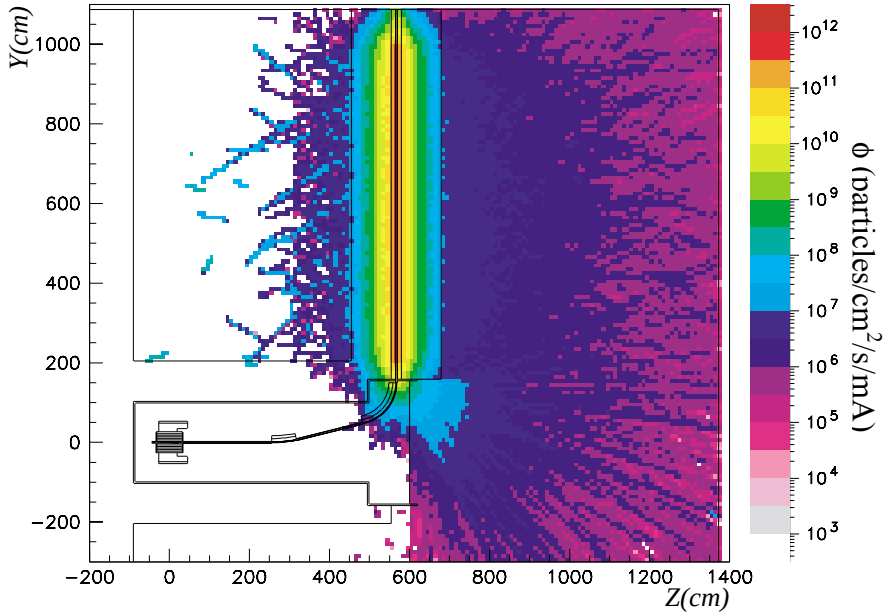

Figure 11 - Particle flux distribution (particle/cm^2/s/mA) due to beam losses along the beam line.

The energy spectra of neutrons and photons escaping the beam tube and the concrete shielding is plotted in Figure 12.

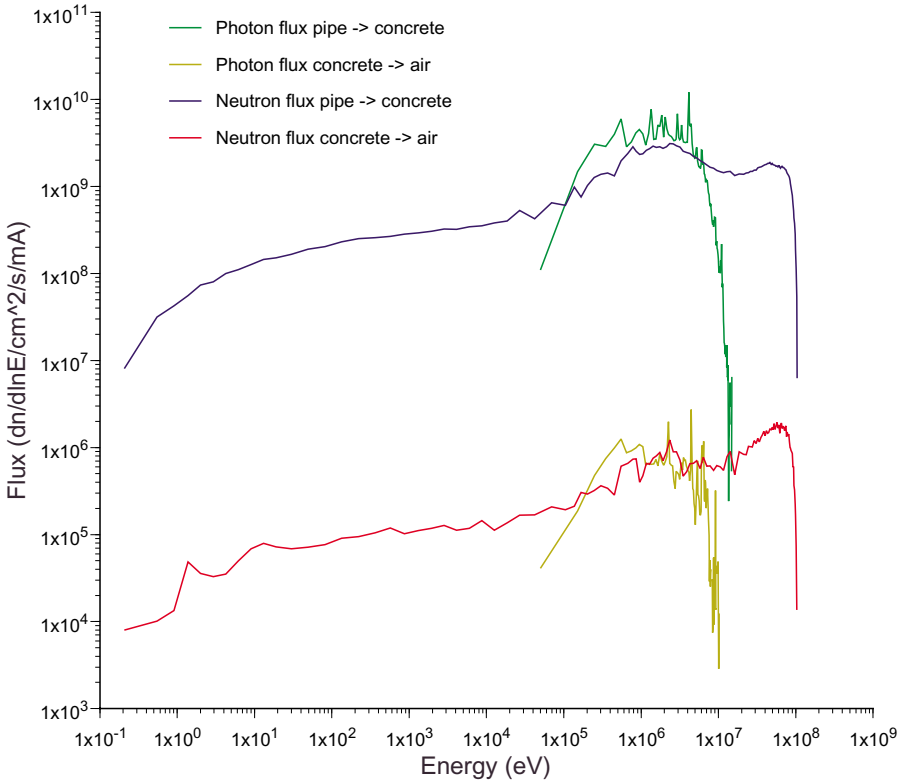

Figure 12 - Energy spectra for photons and neutrons escaping the concrete shielding during normal operation.

These neutrons with energy ranging from a few eV up to 50 MeV will either multiply in concrete through (n, xn) reactions or be captured in most of the cases in boron and barium (see Table V). A small fraction will eventually escape, therefore contributing to the dose rate in the accessible area of the reactor building.

Table V - Integrated neutron flux, heating and damage (per 10 nA of beam loss) in the beam transport tube and surrounding concrete shield structures due to neutrons with energy below 20 MeV.

Region	Flux ($n/cm^2.s$)	Heat (W/cm^3)	DPA/yr
Beam tube	$7.9x10^{5}$	–	–
Concrete	$1.7x10^{4}$	$3.8x10^{-10}$	$1.4x10^{-10}$
Escapes	$3.8x10^{1}$	$7.1x10^{-21}$	$3.2x10^{-13}$
Neutron Absorption		Main Nuclear Reactions	
		Capture	6.50 %
Beam tube	0.09 %	(n, xn)	1.60 %
Air gap	0.02 %	α prod.	88.75 %
Concrete	99.89 %	H prod.	3.06 %
		D prod.	0.06 %
		T prod.	0.003 %

MC calculations show that the particle flux at the surface of the concrete shielding is estimated to be $\phi \approx 10^7$ $n/cm^2/s/mA$, consisting mostly of neutrons, $\phi_n \approx 8\times10^6$ $n/cm^2/s/mA$ and photons, $\phi_\gamma \approx 2\times10^6$ $\gamma/cm^2/s/mA$. The effective dose to human body was calculated using Pelliccioni conversion coefficients [9], resulting in an effective dose of about 3 mSv/s/mA, essentially due to neutrons (90% of the total). Assuming beam losses of 10 nA (1 nA/m × 10 m), we obtain the corresponding dose rate of 100 μSv/h (at contact), which is a 10 times the allowable dose rate in the reactor building for unlimited duration exposures of personnel (10 μSv/h).

This dose rate can be reduced by increasing the thickness of the concrete shielding. For instance, increasing the shielding thickness by 40 cm will reduce the dose rate by one order of magnitude (~ 10 μSv/h), as shown in Figure 13.

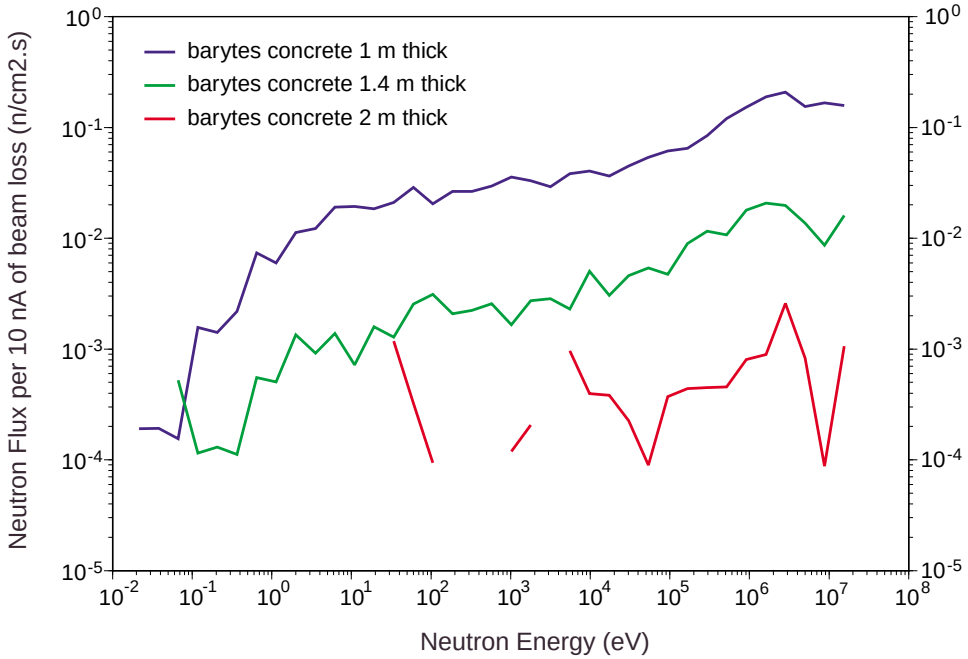

Figure 13 - Variation of the escaping neutron flux as a function of the thickness of the shielding.

The composition of the concrete also has an important role in the effective dose. Different types of concrete have been simulated and the flux of neutrons escaping the shielding is illustrated in Figure 14.

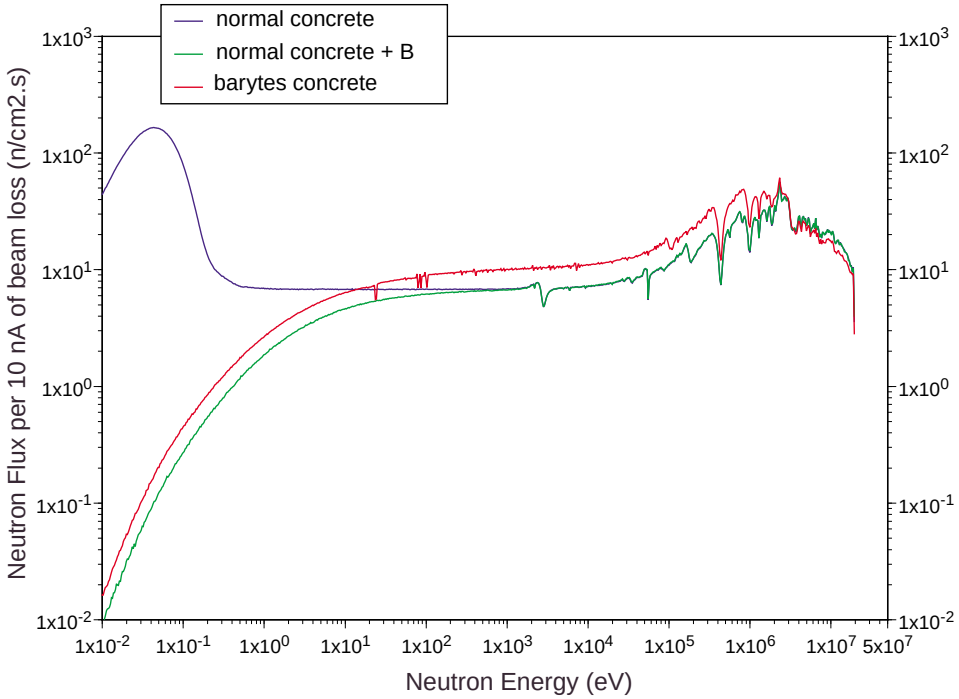

Figure 14 - Energy spectra of neutrons in the center of the shielding for different concrete compositions.

Further shielding options were analysed; the results from the dose calculations are summarised in Table VI. The effective doses at the surface of the shielding and at 5 m from the shielding surface (corresponding approximately to the distance of the control room from the beam line) are reported.

Table VI - Effective dose on the surface of the shielding and at 5 m from the same surface, for a beam loss of 1 nA/m along the 10 m of beam line (straight section), for the different shielding configurations analysed.

Beam pipe	Shielding Configuration	Effective dose at the surface (μSv/h)	Effective dose 5m from the surface (μSv/h)
8 mm Al	1 m normal concrete	350	64
8 mm Al	1 m baritic concrete	100	18
8 mm Al	1.4 m baritic concrete	9.5	2.4
8 mm AISI304	1.4 m baritic concrete	7.9	1.8
2 mm Al	1.4 m baritic concrete	8.3	1.9
2 mm AISI304	1.4 m baritic concrete	7.5	1.7
8 mm AISI304	20 cm Fe, 1.2 m baritic concrete	3.7	0.8
8 mm AISI304	20 cm Cu, 1.2 m baritic concrete	3.2	0.8
2 mm Al	20 cm Cu, 1.2 m baritic concrete	3.9	0.9
2 mm Al	5 cm Cu, 15 cm borated poly, 1.2 m baritic concrete	10.5	2.4
2 mm Al	20 cm borated poly, 1.2 m baritic concrete	10.8	2.5
2 mm AISI304	2 m baritic concrete	0.4	0.12
8 mm AISI304	20 cm Fe, 1.8 m baritic concrete	0.2	0.06
8 mm AISI304	20 cm Cu, 1.8 m baritic concrete	0.2	0.06

The present analysis has shown that it is possible to reduce the effective dose due to beam losses in normal operating conditions below the limit of 10 μSv/h.

This reduction is achieved primarily by increasing the thickness of the concrete shielding. For instance, increasing the thickness by 1 m reduces the dose rate by more than two orders of magnitude.
The presence of boron and barium in the concrete is also very important (it reduces the dose rate by nearly a factor 4).
Further reduction of the dose rate can be obtained by changing the composition and thickness of the beam tube. A pipe made of stainless steel can potentially decrease the dose by another 10 – 15 %.
Inserting different Cu or Fe layers can further improve the dose rates emitted at the surface of the concrete shielding. For example, with a 20 cm thick copper or iron layer surrounded by 1.8 m of baritic concrete, the effective dose at the surface is about 0.2 μSv/h, which is below the maximum allowable dose rate. However, the improvement in the effective dose is achieved at the expense of an increase in activation, as well as in the overall weight of the beam line shielding.
Given the above considerations, the layout consisting of 1.4 m of baritic concrete, with a 2 mm thick AISI304 beam pipe (blue line in Table VI) can be adopted as a reference configuration, resulting in an effective dose at the surface of the shielding of the about 8 μSv/h for 1 nA/m beam losses at 1 mA proton current. However, the maximum beam current envisaged during the TRADE experiment will be ~ 0.25 mA in order not to exceed the limit of 50 kW of beam power imposed by the thermal-hydraulic requirements of the spallation target. Consequently, an additional factor 4 should be applied to the doses reported in Table VI, resulting in a dose at the surface of 2 μSv/h for the reference case.
Figure 15 represents the effective dose as a function of the radial distance from the beam pipe for a beam current of 0.25 mA and 10^{-5} beam losses (0.25 nA/m of beam losses along 10 m of straight section).

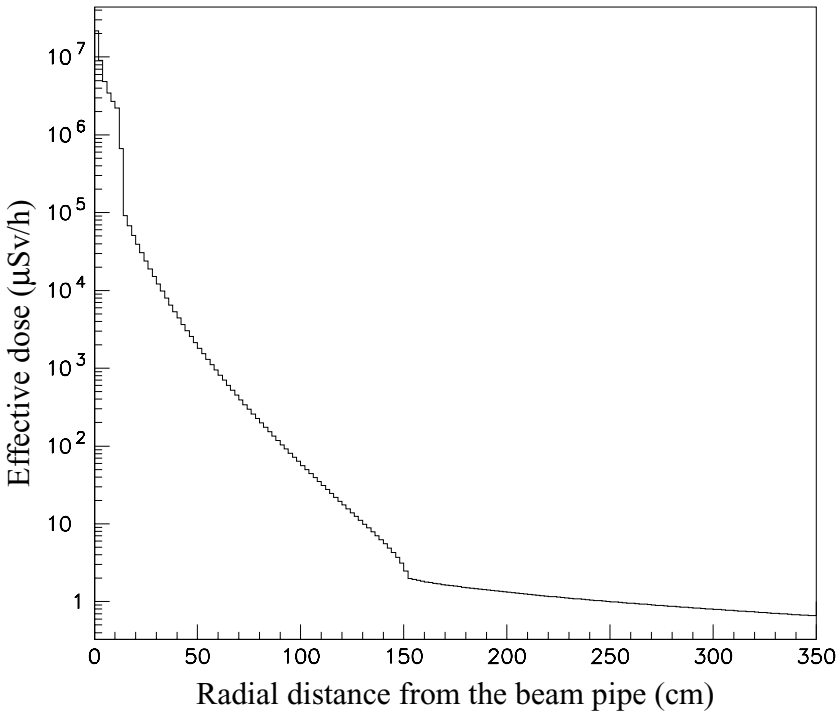

Figure 15 - Effective dose as a function of the radial distance to the beam pipe for a beam current of 0.25 mA and 10^{-6}/m beam losses for the reference configuration.

In conclusion, the effective dose obtained for the reference configuration satisfies the safety requirements (at least for the straight section). Moreover, one should also consider that the calculation scheme adopted is a pessimistic one since we have used a user defined source routine which generates 110 MeV protons distributed along the length of the beam tube at a radius of 1.6 cm and propagated outwards, i.e. perpendicular to the beam pipe. In reality, the protons exiting the beam line will have a very small angle, and therefore will be attenuated even more. Indeed, we have checked that the reduction factor assuming a divergence of 17 mrad (i.e. 1º) is of 2.5, reducing the effective dose at the surface of the shielding to about 0.8 μSv/h.

7. TARGET AND BEAM-LINE ACTIVATION

The neutron flux spectra generated by the EA-MC code package can be used to estimate the heating and damage to structural materials by neutrons with energy above and below 20 MeV. Indeed, in TRADE one can consider separately the high-energy portion of the spectrum, due to the primary proton shower, with its intensity proportional to the beam current, and a lower energy region associated with the fission-multiplying medium, proportional to the reactor power.
Table VII reports results of damage and heating calculations. An accurate calculation is made by using the detailed geometric model of the device and by computing the neutron-induced damage self-consistently in each geometric element (made by a given material) for each interacting nuclide [10].

Table VII -Integrated flux, heating and damage of the spallation target unit internal structures, due to low-energy neutrons (LE) and high-energy particles (HE) as computed by EA-MC and FLUKA

Region	**Flux (part/cm^2.s)**		**Heat (W/cm^3)**		**DPA/year**	
	HE	LE	HE	LE	HE	LE
Proton beam tube (Al)	$5x10^{11}$	$2.7x10^{10}$	$5x10^{-2}$	–	$9.9x10^{-3}$	–
Spallation target (W)	$8x10^{13}$	$3.5x10^{13}$	≥ 100	$2.1x10^{-1}$	22.2	5.5
Spallation target vessel (Al)	$7x10^{12}$	$2.4x10^{13}$	0.5	$1.1x10^{-1}$	$1.4x10^{-1}$	2.3
Water Coolant	$5x10^{12}$	$4.1x10^{12}$	$5x10^{-2}$	$2.6x10^{-3}$	$2.3x10^{-2}$	$3.7x10^{-2}$

Burnup calculations have been carried out to estimate the activation of the tungsten spallation target and its aluminium supports. As shown in Figure 16, it is worth noting that the activity of the spallation target (expressed in Ci/mA.yr) is dominated by activation resulting from successive thermal neutron captures during the first year. After one year the activity is dominated by the decay of the spallation products, mostly Ta, Lu and Hf isotopes. At longer times (> 40 years) tritium and ^{90}Sr are the only isotopes of importance. Note that tritium is the only volatile isotope produced in the spallation target.

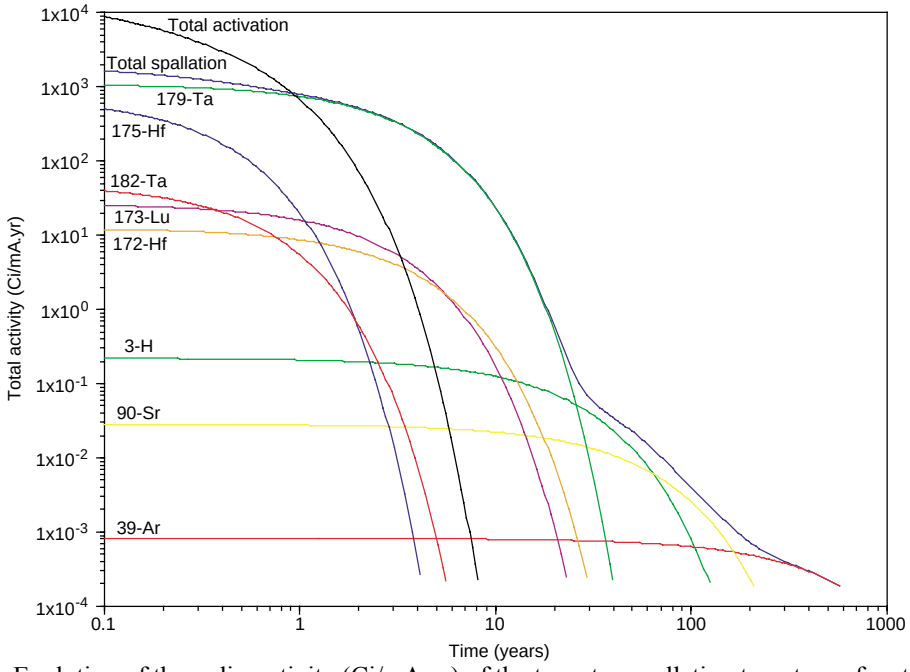

Figure 16 -. Evolution of the radio-activity (Ci/mA.yr) of the tungsten spallation target as a function of time.

Similarly, Figure 17 shows that the activity of the aluminium beam tubes is entirely dominated by tritium and ^{22}Na. The level of radio-activity is however 1/100000 the one of the spallation target.

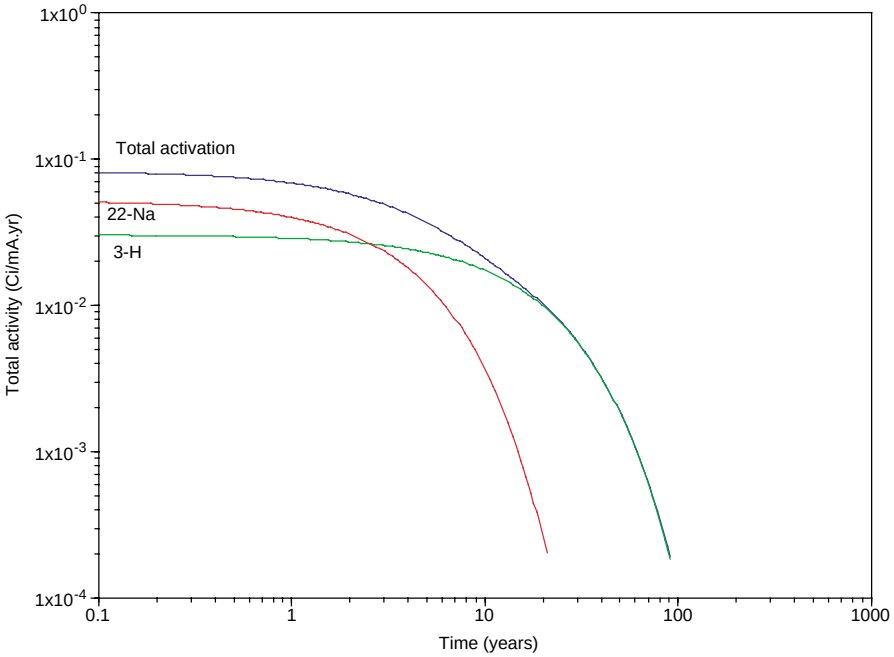

Figure 17 -. Evolution of the radio-activity (Ci/mA.yr) of the aluminium beam tubes as a function of time.

Concerning the activation of the water contained around the beam tube, burnup calculations have been carried out to estimate the activation of the water contained around the beam tube, due to losses occurring during normal operations. As shown in Figure 18, it is worth noting that the activity of the water volume 10 cm from the beam line (expressed in µCi/cm^3/mA.yr) is dominated by the decay of the spallation products, mostly ^{7}Be (8×10^{-4} µCi/cm^3/mA.yr). After one year tritium and ^{14}C are the only isotopes of importance. Note that tritium is the only volatile isotope produced in water.

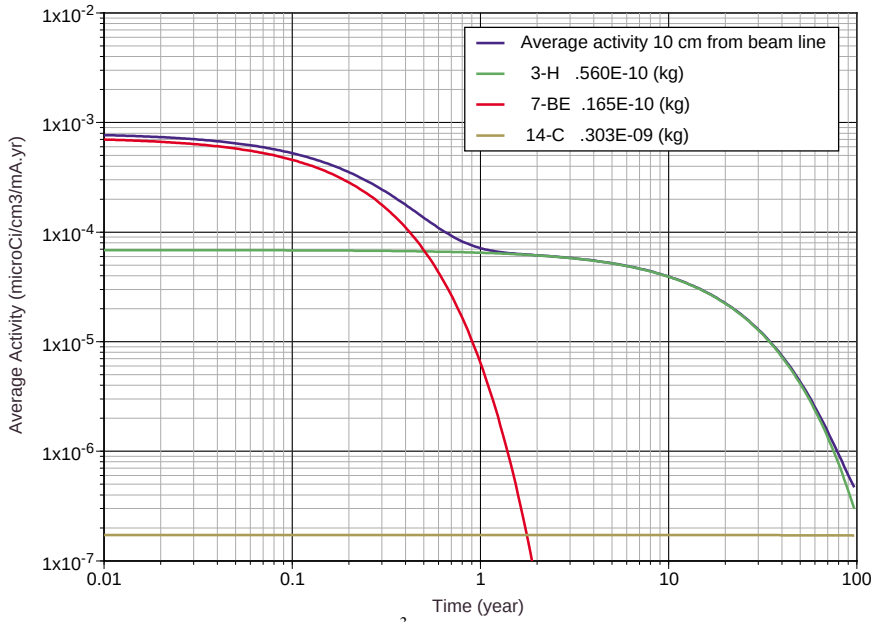

Figure 18 - Evolution of the radio-activity (µCi/cm^3/mA.yr) of water 10 cm from the beam line due to normal beam losses (1 nA/m of beam losses along 6 m of straight section).

8. REPRESENTATIVITY OF THE EXPERIMENT

Some reactivity insertion transients have been simulated by the TIESTE-MINOSSE code [8]. Three different subcriticality levels (-3.81$, -1.74$ and –0.72$, with 1$ ~ 700 pcm for TRIGA) were assumed for the analysis. The power level was 200 kW at the transient beginning. The fuel temperature feedback effects were taken into account. Figure 19 shows the power transients induced by a reactivity linear ramp of 50 cents in 2 s for the three subcritical levels considered. For sake of comparison, the response of a Pb/Bi cooled experimental 100 MW_{th} XADS [1] to the same reactivity insertion is shown in the figure. The influence of different thermal feedback impacts on power allow to evaluate in what extent feedback effects on the experimental power transients will decrease by decreasing the multiplying system effective multiplication factor, K_{eff}.

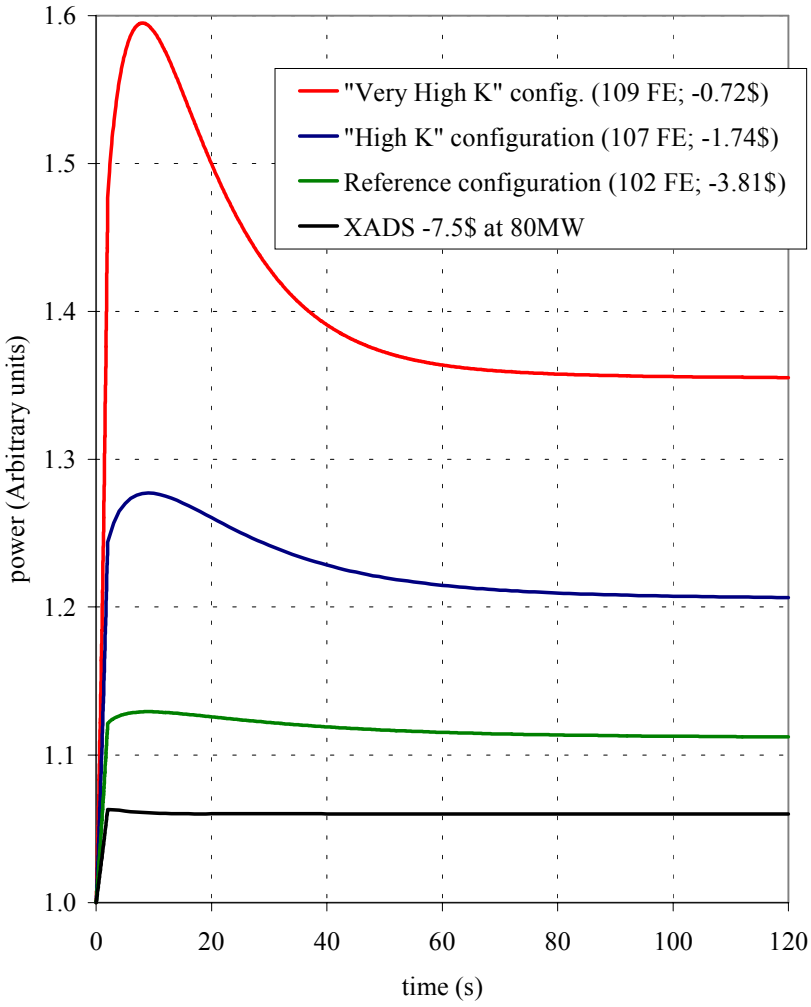

Figure 19 - Normalized-power transients induced by reactivity insertion (50 cents in 2s) for different TRADE configurations.

Results indicate that TRADE experiments performed by configurations closer to the criticality conditions will be representative of the ADS dynamics relevant to higher power systems.
As far as the spectrum, TRADE will bring essential demonstration elements, valid for any type of ADS, e.g. with fast spectrum. In fact, although the kinetics parameters of a TRIGA (β_{eff} ~ 0.007, Λ_{eff} ~ 10^{-4} s) and a fast spectrum ADS like XADS (β_{eff} ~ 0.003, Λ_{eff} ~ $0.5 \cdot 10^{-6}$ s) are very different, the dynamic response to perturbations are very similar.

CONCLUSIONS

By means of 3-D Monte Carlo simulations codes a number of neutronic features of the proposed TRADE experiment have been analysed. Realistic models of some in-vessel structures, which may affect the overall neutronics, have been included in the simulations. Simplified dynamic codes were used to evaluate the dynamic behaviour of the TRADE subcritical core to some reactivity insertion transients.
The results show that the desired sub-criticality levels and power distributions can be achieved. In particular, TRADE allows to investigate a significant range of subcriticality levels, going from 0.90 (source dominated) to near critical. Assuming 200 kW as core power, the corresponding accelerator current, of the order of ~ 0.5 mA for K=0.90 and 0.07 mA for K=0.99, produces a power in the target that can be easily evacuated.
The dynamic neutronic conditions that can be experimentally realized in TRADE are well representative of dynamic ADS behaviour at higher powers [11]. In particular, the results shown in Section 6 indicate that TRADE will validate the transition between the source and the feedback dominated dynamic behaviour of an ADS. Finally, recent studies [2] performed at Argonne National Laboratories indicate that the dynamic response of a fast spectrum reference ADS of several hundreds MW to, e.g., reactivity insertions, is matched, as general behaviour, by the responses obtained in a thermal spectrum subcritical system, to similar reactivity insertions.
All these considerations allow to consider TRADE as a full scale demonstration of the ADS concept, in particular for what concerns the dynamic behaviour of the system.

REFERENCES

1. The European Technical Working Group on ADS, "A European Roadmap for Developing Accelerator Driven System (ADS) for Nuclear Waste Incineration", April 2001, www.enea.it.
2. D. G. Naberejnev, M. Salvatores, G. Palmiotti, F. G. Kondev, G. Imel, T. Bauer and Frank Harmon, "Possible experiment for study of the ADS dynamics", *This Conference*.
3. M. Salvatores et al., "MUSE-1: a first experiment at MASURCA to validate the physics of sub-critical multiplying systems relevant to ADS", *Proc. of 2nd ADTT Conference*, Kalmar, Sweden, June 1996.
4. L. Zanini, A. Ferrari, A. Herrera-Martínez, Y. Kadi, C. Rubbia, N. Burgio, M. Carta, A. Santagata, L. Cinotti, "Radioprotection calculations for the TRADE experiment", *NEA Nuclear Science Committee*, *Third International Workshop on the Utilisation and Reliability of High Power Proton Accelerators*, Santa Fe, New Mexico, May 12-16, 2002.
5. C.Rubbia et al., "Conceptual design of a fast neutron operated high power Energy Amplifier", CERN report CERN/AT/95-44 (EET), Geneva, September 29, 1995.
6. Y.Kadi et al., "The EA-MC Monte Carlo Code Package", *Proc.of the Fifth International Meeting on Simulating Accelerator Radiation Environment —SARE-5:Models and Codes for Spallation Neutron Sources"*, OECD Headquarters, Paris, France, July 17-18, 2000.
7. Judith F.Briesmeister, Editor, "MCNP TM -A General Monte Carlo N-Particle Transport Code, Version 4C", Los Alamos National Laboratory report LA-13709-M, March 2000.
8. A. D'Angelo, G. Bianchini, M. Carta, P. Bosio, P. Ravetto, M. M. Rostagno, "A simple model to evaluate the natural convection impact on the core transients in Liquid Metal Cooled ADS", *Proc. of 6th OECD/NEA Information Exchange Meeting on Actinide and Fission Product Partitioning and Transmutation*, Madrid (Spain), December 11-13, 2000.
9. A. Ferrari and M. Pelliccioni, "Dose equivalents for mono-energetic electrons incident on the ICRU sphere", *Radiation Protection Dosimetry*, **55** n°3, 207-210 (1994) (also LNF-94/005 (P) (1994)).
   "Fluence to dose equivalent conversion data and effective quality factors for high energy neutrons", *Radiation Protection Dosimetry* **76**, n°4, 215-224 (1998).
10. F. Carminati and Y. Kadi, "Implementation of a new Routine for Damage Calculations for the EA Monte Carlo", CERN internal report, CERN/LHC/EET 98-004, Geneva, April 20, 1998.
11. M. Salvatores, A. D'Angelo, D. Naberejnev, " The demonstration of the ADS concept ", *NEA Nuclear Science Committee*, *Third International Workshop on the Utilisation and Reliability of High Power Proton Accelerators*, Santa Fe, New Mexico, May 12-16, 2002.